

# To Glue or Not to Glue? Classical vs Learned Image Matching for Mobile Mapping Cameras to Textured Semantic 3D Building Models

Simone Gaisbauer\*, Prabin Gyawali\*, Qilin Zhang, Olaf Wysocki, Boris Jutzi

Professorship of Photogrammetry and Remote Sensing, TUM School of Engineering and Design,  
Technical University of Munich, 80333 Munich, Germany

(simone.gaisbauer, prabin.gyawali, qilin.zhang, olaf.wysocki, boris.jutzi)@tum.de

\*Authors equally contributed

**Keywords:** Feature matching, handcrafted features, learnable features, textured CityGML models, LoD2, visual localization

## Abstract

Feature matching is a necessary step for many computer vision and photogrammetry applications such as image registration, structure-from-motion, and visual localization. Classical handcrafted methods such as SIFT feature detection and description combined with nearest neighbour matching and RANSAC outlier removal have been state-of-the-art for mobile mapping cameras. With recent advances in deep learning, learnable methods have been introduced and proven to have better robustness and performance under complex conditions. Despite their growing adoption, a comprehensive comparison between classical and learnable feature matching methods for the specific task of semantic 3D building camera-to-model matching is still missing. This submission systematically evaluates the effectiveness of different feature-matching techniques in visual localization using textured CityGML LoD2 models. We use standard benchmark datasets (HPatches, MegaDepth-1500) and custom datasets consisting of facade textures and corresponding camera images (terrestrial and drone). For the latter, we evaluate the achievable accuracy of the absolute pose estimated using a Perspective-n-Point (PnP) algorithm, with geometric ground truth derived from geo-referenced trajectory data. The results indicate that the learnable feature matching methods vastly outperform traditional approaches regarding accuracy and robustness on our challenging custom datasets with zero to 12 RANSAC-inliers and zero to 0.16 area under the curve. We believe that this work will foster the development of model-based visual localization methods. Link to the code: [https://github.com/simBauer/To\\_Glue\\_or\\_not\\_to\\_Glue](https://github.com/simBauer/To_Glue_or_not_to_Glue)

## 1. Introduction

Feature matching is one of the fundamental tasks in mobile mapping with applications ranging from image registration, structure-from-motion, and 3D reconstruction to visual localization. The ability to reliably detect, describe, and match keypoints between images is crucial for robustness in these tasks. Traditional, handcrafted, local feature descriptors such as Scale-Invariant Feature Transform (SIFT) (Lowe, 2004), SURF (Bay et al., 2006), and Oriented FAST and Rotated BRIEF (ORB) (Rublee et al., 2011) have been used extensively due to their robustness to geometric and photometric transformations. With the advancements in deep learning, learnable feature extractors and *matchers*, such as SuperPoint (DeTone et al., 2018), SuperGlue (Sarlin et al., 2020), LightGlue (Lindenberger et al., 2023), and LoFTR (Sun et al., 2021), have demonstrated superior performance in challenging scenarios by leveraging data-driven feature representations and sophisticated matching strategies.

Amid the growing adoption of learnable feature-matching methods, there is still a lack of comprehensive evaluation that systematically compares their performance against classical methods in the specific context of camera-to-model image matching for visual localization. Whilst only a few studies specifically evaluate different feature-matching methods for model-based visual localization (Panek et al., 2022), numerous works provide evaluations on generic benchmark datasets or on the accuracy of feature matching itself (Bian et al., 2018; Karpur et al., 2024). Additionally, learnable methods typically require higher computational resources, making it necessary to assess their trade-offs in terms of efficiency and accuracy.



Figure 1. Classical (top) vs learnable (bottom) feature matching methods on a 3D building model’s (left) texture image (middle, red rectangle) to mobile mapping image (right) with green lines connecting inlier matches (<30 px projection error).

This study aims to bridge this gap by systematically comparing classical and learnable feature-matching methods and evaluating them on standard benchmarks and domain-specific datasets of mobile mapping images and textured semantic 3D building models. Our contributions are summarized as follows:

- We propose a framework for mobile mapping pose estimation based on textured semantic 3D models
- We comprehensively analyze the impact of classical and novel image-matching methods on both standard benchmarks and custom vehicle and drone data

- We extend the TUM2TWIN data for the camera-to-model use case validation

## 2. Related Works

Methods for feature matching are a well-studied topic in the computer vision and photogrammetry domains. We refer to the recent surveys, such as Huang et al. (2024); Xu et al. (2024), for a comprehensive overview of classical and learnable feature matching methods. Hereafter, we focus on the relevant research in visual localization using 3D models and camera images.

### 2.1 Semantic 3D Building Models

We follow the definition of Wysocki et al. (2024); Kolbe and Donaubauer (2021) that defines *semantic 3D building models* as building representation combining object-level geometry with semantic information within a hierarchical data structure, explicitly defining relationships between objects. They typically adhere to the CityGML standard (Gröger et al., 2012) and use watertight geometry, allowing for volumetric space understanding through accumulating outer-observable surfaces in a boundary representation (B-Rep). Nowadays, we observe increasing availability of textured semantic 3D building models (Wysocki et al., 2024) at level of detail (LoD)1 (cuboid shape) and LoD2 (cuboid shape complemented by complex roof structure), which also follow piece-wise planar geometry. Unlike virtual reality models, where 3D meshes with appearance attributes represent geometry, semantic models provide structured, interpretable data (Kolbe and Donaubauer, 2021).

### 2.2 Feature Matching for Localization

Various approaches to 6 DoF pose estimation using images and a world reference geometry exist, with the main differences in the type of reference, matching strategy, the requirement of coarse alignment, and the targeted applications. A well-established reference for visual localization are Structure-from-Motion models and posed images (Mueller et al., 2019), for example, used by the Visual Localization benchmark (Sattler et al., 2018). Promising results of learnable feature-matching methods for visual localization using rendered views of dense 3D mesh models as reference have been published (Panek et al., 2022). Furthermore, the authors evaluate their method Mesh-Loc on coarser textured and untextured 3D mesh and CAD models and showed that the performance is superior for the more detailed models (Panek et al., 2023). Evaluating image-to-model feature matching with rendered images of untextured CityGML models for improving GNSS/IMU positioning in urban areas are known (Bieringer et al., 2024). They also conclude that higher levels of detail are favourable for the task. Projections of semantic city models also serve as the reference for visual localization in (Loeper et al., 2024). Their approach to deal with low LoD is to match lines instead of local features.

## 3. Methodology

We first describe the selection of methods, followed by introducing the underlying geometric model. After testing the methods on the generic datasets, we introduce our own 3D model texture and camera image pairs to the pipeline. All involved stages are discussed in this section since it is not a standard evaluation procedure for feature-matching methods. Figure 2 shows the general outline.

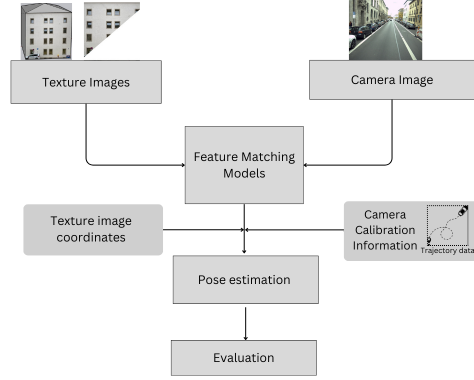


Figure 2. Camera-to-textured-model image matching overview.

We evaluate the facade texture and camera image matching by absolute pose estimation. We can derive world coordinates for the matched facade keypoints as the texture images are geo-referenced by being warped on model faces with known world coordinates. Since we know the world coordinates for the matched pixels in the camera image, we can estimate the absolute camera pose using a Perspective n-Point (PnP) algorithm (Li et al., 2012). This estimate is then evaluated using the ground-truth camera poses.

### 3.1 Feature Matching Methods

We compare well-adopted methods from both the classical and learnable domains. At the same time, we choose them to be well-balanced in terms of the method and theory that the models utilize. Table 1 lists the selected models.

Category	Extractor	Matcher
Classical	SIFT	FLANN
	ORB	NN
	AKAZE	NN
Learnable	Super Point	Super Glue
	Super Point	Light Glue
	DISK	Light Glue
	LoFTR	

Table 1. Selected feature matching models.

**3.1.1 Classical Methods** With the term *classical*, we refer to handcrafted features, which were mainly developed in the pre-deep-learning era of photogrammetry and computer vision. All three chosen methods rely on the pipeline of feature detection, description and matching. The type of detectors varies with ORB (Rublee et al., 2011) as intensity-based, and SIFT (Lowe, 2004) and Accelerated-KAZE (AKAZE) (Alcantarilla and Solutions, 2011) as blob-type features. The detectors are combined with their associated descriptors, which are binary in the case of ORB and AKAZE. All descriptors are invariant to rotation, and SIFT and AKAZE additionally to scale. When referring to SIFT, we actually are using RootSIFT, which is recommended by Arandjelović and Zisserman (2012).

The *matchers* for the classical methods are all based on computing nearest neighbours on the detected features’ descriptors. For the SIFT features, we use a faster approximation from the Fast Library for Approximate Nearest Neighbors (Muja and Lowe, 2009) (FLANN) in order to account for the descriptors’ higher computational complexity. For ORB and AKAZE, we

use brute-force nearest neighbours (NN) matching. The neighbourhood metric is the Euclidean norm for SIFT and the Hamming distance for the binary descriptors.

**3.1.2 Learnable Methods** For the learnable methods, we evaluate four models. The first three pipelines are two-step approaches, which extract features (*extractors*) in the first step and match them in the second one. Feature extraction is done either with SuperPoint (DeTone et al., 2018) or DISK (Tyszkiewicz et al., 2020) and matching either with SuperGlue (Sarlin et al., 2020) or LightGlue (Lindenberger et al., 2023). The fourth method, LoFTR (Sun et al., 2021), is a holistic *matcher*, which directly determines matches from input image pairs.

Both DISK and SuperPoint use fully-convolutional neural networks (CNN) as architectures. Whereas DISK is trained in a weakly supervised manner, SuperPoint is self-supervised. DISK is trained on a COLMAP-posed selection of MegaDepth images. It uses reinforcement learning informed by the matchability of the features across two images. SuperPoint uses two-step training on synthetic shapes and MS COCO 2014 (Lin et al., 2014) images warped using synthetic homographies.

The *matchers* SuperGlue and LightGlue both use transformers, with the difference that LightGlue is an advanced, lighter and more efficient version of SuperGlue, as it uses the dynamic attention based on confidence. LoFTR instead performs feature extraction and detection in one step by chaining a CNN with their attentional Local Feature Transformer module. According to the authors, the one-step method should be beneficial for limited texture (Sun et al., 2021). We use the outdoor models of all three *matchers*, which are trained on Megadept (Li and Snavely, 2018) images.

## 3.2 Extracting Images for Matching

The first step is to acquire the texture images and their relevant geo-information from the models. The second step is to extract corresponding images captured by the mobile camera and their poses from the survey data. This step is not straightforward due to the compatibility of the data formats and reference systems discussed in Section 6.

**3.2.1 Texture Images of 3D Models** Even though usually all faces of the semantic 3D building models are textured, it is desired to filter the images for the street-facing facades and also consider their quality (example shown in Figure 3). Since each texture image is associated with one planar, polygonal face of the model, highly detailed facades can lead to minor and non-meaningful image patches, e.g., the right building part in Figure 3. Therefore, texture images below a certain size and with more prominent absent optical information are not taken into consideration. The obtained images are used to create image pairs with the camera images for a particular building facade.



Figure 3. Exemplary textured semantic 3D building model.

For the selected texture images, the respective coordinates of the polygonal ring adhere to the standard CityGML models, which can be adapted to other encodings. Converting between world coordinates and pixels is done via coordinate system transformations (Figure 4). In addition to the common pixel coordinate system, each texture image is associated with a so-called st-coordinate system, which maps the image to the polygonal face and links to the world coordinates (Gröger et al., 2012, p. 40f, *ParameterizedTexture*). The world coordinates are given in two horizontal plus one vertical component as East, North, and Up (E, N, U).

For all images, the values of the associated face’s edge st-coordinates (attribute *textureCoordinates*) of *TexCoordList* class) and world coordinates (attribute *posList* of *LinearRing* class) are extracted from the semantic 3D models faces and stored. The following approach is used to compute the world

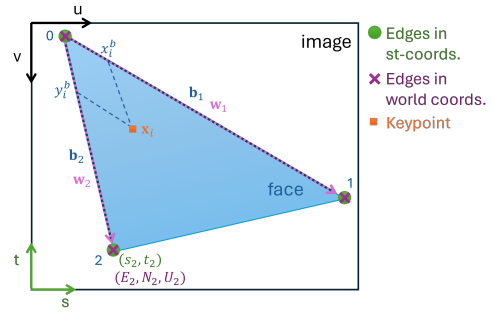


Figure 4. Sketch of the texturing, coordinate systems and coordinate conversion.

coordinates of any pixel in the texture image from the stored edge information (Figure 4). First, the pixel location of the  $i$ -th feature  $(u_i, v_i)^T$  with  $u \in [0, width]$ ,  $v \in [0, height]$  is converted to st-coordinates  $(s_i, t_i)^T$  with  $s \in [0, 1]$ ,  $t \in [0, 1]$ .

$$s_i = u_i / width; \quad t_i = 1 - v_i / height, \quad (1)$$

As the edges (index  $j = 0, \dots, N_{edges} - 1$ ) are given both in st-coordinates  $\mathbf{x}_j^s$  and world coordinates  $\mathbf{x}_j^w$ , we can construct a face-aligned basis  $\mathbf{b}$  in 2D and its 3D metric equivalent  $\mathbf{w}$  through the vectors along two vertices starting at one edge.

$$\mathbf{b}_1 = \mathbf{x}_1^s - \mathbf{x}_0^s; \mathbf{b}_2 = \mathbf{x}_2^s - \mathbf{x}_0^s \quad (2)$$

$$\mathbf{w}_1 = \mathbf{x}_1^w - \mathbf{x}_0^w; \mathbf{w}_2 = \mathbf{x}_2^w - \mathbf{x}_0^w \quad (3)$$

Then, the st-coordinates of the keypoint  $\mathbf{x}_i^s$  are transformed from st-coordinates to the face-aligned intermediate  $\mathbf{b}$ -basis.

$$\mathbf{x}_i^b = \mathbf{A}^{-1}(\mathbf{x}_i^s - \mathbf{x}_0^s), \text{ with: } \mathbf{A} = \begin{pmatrix} b_{1,1} & b_{2,1} \\ b_{1,2} & b_{2,2} \end{pmatrix} \quad (4)$$

Finally, world coordinates  $\mathbf{x}_i^w = (E_i, N_i, U_i)^T$  are obtained by scaling this intermediate representation  $\mathbf{x}_i^b = (x_i^b, y_i^b)^T$  with the vertex vectors in world coordinates  $\mathbf{w}$ .

$$\mathbf{x}_i^w = \mathbf{x}_0^w + x_i^b \cdot \mathbf{w}_1 + y_i^b \cdot \mathbf{w}_2 \quad (5)$$

One advantage of this method is that it is also compatible with images where the texture of the facade face does not cover the whole extent of the image.

**3.2.2 Camera Images** The format for the camera poses and calibration matrix as input to the evaluations is described below. The  $3 \times 4$  transformation matrix  $\mathbf{T}_w^c$  to convert homogeneous world coordinates to the camera frame contains the  $3 \times 3$  rotation matrix  $\mathbf{R}_w^c$  to rotate coordinates from the world to camera frame and the translation  $\mathbf{t}_{cw}^c$  as the world origin relative to the camera origin expressed in the camera frame.

$$\mathbf{T}_w^c = [\mathbf{R}_w^c | \mathbf{t}_{cw}^c] = [\mathbf{R}_w^c | -\mathbf{R}_w^c \mathbf{t}_{wc}^w] \quad (6)$$

The calibration matrix is the  $3 \times 3$  matrix that transforms the depth-normalized coordinates on the unit plane to homogeneous image coordinates in pixels by scaling with the focal length  $f$  and shifting with the focal point  $c$ . The image coordinate system is left-upper corner fixed as visualized in Figure 4 ( $u$ -component is now  $x$  and  $v$  is  $y$ ).

$$\mathbf{K} = \begin{pmatrix} f_x & 0 & c_x \\ 0 & f_y & c_y \\ 0 & 0 & 1 \end{pmatrix} \quad (7)$$

**3.2.3 Image Pairs for Matching** The creation of image pairs for matching involves the selection and filtering of camera images that correspond to the 3D model facade. All the camera images that contain one facade element are referenced as pairs. The final image pairs consist of associated facade images, corresponding camera images, their respective camera parameters, and ground truth poses. One facade image can be matched to several camera images from different cameras, positions and viewing angles. This gives the opportunity to test whether the feature matches these varying conditions. The final image pairs are passed through the models to evaluate the matching and pose estimation performance.

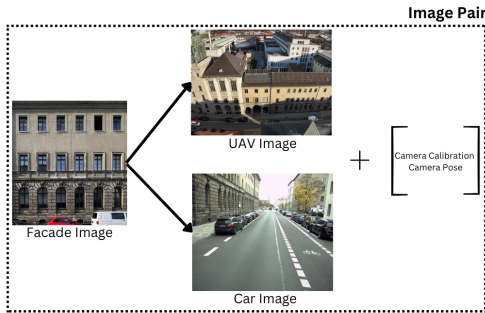


Figure 5. All the camera images that contain one facade element are referenced as pairs.

### 3.3 Camera-to-Textured-3D-Model

As previously discussed, we know the world coordinates of the correctly matched pixels in the facade images from the model information (Section 3.2.1) and the absolute pose and calibration of the camera (Section 3.2.2). Therefore, we can evaluate the performance of the feature matching method on facade texture-camera image pairs with the absolute pose as their geometric relationship.



Figure 6. Example image of a textured 3D model.

**3.3.1 Pose Estimation** The pose estimation is done using Perspective-n-Point with RANSAC outlier removal. Instead of testing a range of values, we set the RANSAC threshold  $t$  to a fixed value. The parameter is chosen according to the inconsistencies of the model and camera data, which we further discuss in Section 6. In order to use the PnP algorithm on geo-referenced geospatial data, we need to account for the large and variable magnitudes of our coordinates and of the translation. Therefore, we center the world coordinates of the matched points in the texture images prior to the pose estimation. We store this offset  $\mathbf{x}_{center}$  and later apply it also to the ground truth translation when comparing it to the estimated translation. The formula for applying the offset to the ground truth is:

$$\mathbf{t}_{gt,centered} = \mathbf{t}_{gt} + \mathbf{R}_{gt} \mathbf{x}_{center} \quad (8)$$

## 4. Experimental Setup

### 4.1 Implementation

Our evaluation is built upon the repository Glue Factory<sup>1</sup> (Lindenberger et al., 2023; Pautrat et al., 2023). For our extensions to this code base with additional methods and data sets, we rely on the libraries OpenCV<sup>2</sup> and Kornia<sup>3</sup> (Riba et al., 2020). The pose estimation was done with OpenCV’s Perspective-n-Point<sup>4</sup> implementation with RANSAC outlier removal, while parameter  $t$  of RANSAC set consistently for all methods to 10. We used NVIDIA GeForce GTX 1060 6GB, Intel® Core™ i7-9700-Processor.

### 4.2 Data

We evaluate the methods in two steps: First, we use common evaluation strategies with a generic dataset, and second, we use our custom analysis and dataset.

**4.2.1 Generic Datasets** Following the evaluation by Lindenberger et al. (2023), we tested the classical and learnable methods on common benchmarks, namely HPatches (Balntas et al., 2017) and the Megadepth-1500 (Li and Snavely, 2018) image pairs. The first dataset comprised image sequences whose members can be geometrically related by homographies and vary either in intensity or geometry. The evaluation metric was based on estimated and ground-truth homographies. The second dataset contained 1500 image pairs designed using images from the scenes of St. Peters Square and Reichstag from the larger Megadepth dataset. The geometric ground

<sup>1</sup> <https://github.com/cvg/glue-factory/>

<sup>2</sup> <https://opencv.org/>

<sup>3</sup> <https://kornia.readthedocs.io/en/stable/>

<sup>4</sup> [https://docs.opencv.org/3.4/d5/d1f/calib3d\\_solvePnP.html](https://docs.opencv.org/3.4/d5/d1f/calib3d_solvePnP.html)

truth was given by epipolar geometry and was provided by relative poses computed with the Structure-from-Motion (SfM) pipeline COLMAP (Schönberger and Frahm, 2016).

#### 4.2.2 TUM2TWIN: Our Custom Image-Model Dataset

We extend the evaluation with our application-specific dataset. The texture images of the semantic CityGML LoD2 buildings are from the open-source project TUM2TWIN<sup>5</sup> (Wysocki et al., 2025). The camera images were acquired by a proprietary mobile mapping vehicle platform by 3D Mapping Solutions GmbH with a Real-Time Kinematic (RTK) system. Furthermore, unmanned aerial vehicle (UAV) images from the TUM photogrammetric reconstruction (Anders et al., 2025), which show facade parts, were selected. The horizontal coordinates were given in the ETRS80 frame and were projected to UTM of EPSG:25832.

One set of camera images was captured on a moving car during a mobile laser scanning campaign by the mobile mapping vehicle. We used images from two of the four mounted cameras, which gave the best views of the facades. As both the given camera parameters and poses differ in the notation and definition, we converted them to the standard OpenCV format<sup>6</sup>. We constructed the rotation matrix and translation vector from the provided altitude and trajectory information. The principal operation on the given camera calibration information was to convert the parameters to our image coordinate system definition and to pixels.

The UAV images were posed during the photogrammetric reconstruction with the commercial software Pix4Dmatic (Anders et al., 2025). The following conversion was applied to the global shift of the 3D reconstruction stored in the OPF file, and a height offset of  $\Delta U = -45.66$  m. The latter is caused by different reference ellipsoids used for the height system, which is the former German official ellipsoid Bessel for the models and the global ellipsoid WGS84 for the UAV data. The final datasets consist of 622 pairs for car-texture and 18 pairs for UAV-texture.

#### 4.3 Evaluation Metrics

The evaluation pipeline on the HPatches and Megadepth-1500 datasets is inspired by the evaluation of (Lindenberg et al., 2023). For our datasets, we customized their methods. We used the same settings for image resizing and limited for the top matches. Minor differences are that we always used standard OpenCV estimators with RANSAC for outlier removal, and the resizing for Megadepth-1500 and TUM images is set to 1024 pixels in the larger dimension for the dense *matcher* LoFTR and DISK.

The evaluation of models consists of three main metrics as used by Lindenberg et al. (2023). First, the evaluation of matches using ground truth involves computing the mean precision at different thresholds. Second, RANSAC estimates of the geometric relationship are assessed using mean number of inliers, mean percentage of inliers, the area under the curve (AUC) of the geometric error–recall curve for different thresholds, mean average accuracy (computed as the mean of the AUCs), and the median error. Finally, the evaluation of matches considers the mean number of keypoints and the mean number of matches among the keypoints.

<sup>5</sup> <https://tum2t.win/>

<sup>6</sup> [https://docs.opencv.org/4.x/d9/d0c/group\\_\\_calib3d.html](https://docs.opencv.org/4.x/d9/d0c/group__calib3d.html)

For individual datasets, HPatches is evaluated based on the re-projection error using the ground truth homography and the homography error, defined as the mean reprojection distance of corner pixels. Megadepth-1500 is analyzed through the distance to the epipolar line using the ground truth relative pose (essential matrix) and the relative pose error, which is computed as the maximum angular difference between the estimated and ground truth translation vector and rotation (decomposed from the essential matrix). Lastly, we assess our TUM data using the reprojection error based on the ground truth absolute pose (projection matrix) and the absolute pose error, which measures both rotation (angular) and translation (metric) differences between the estimated camera pose (using the PnP algorithm) and the ground truth camera pose.

### 5. Results

This section presents our results for the evaluation on both generic and our custom datasets.

#### 5.1 Results for the generic data sets

Model	mPrec. @3px	AUC @5px	mInl.	med.Err [px]
SIFT+FLANN	0.94	0.66	151	1.0
ORB+NN	0.55	0.43	45	3.1
AKAZE+NN	0.64	0.56	171	1.6
SP+SG	0.93	0.69	102	1.1
SP+LG	0.94	0.68	102	1.1
DISK+LG	0.97	0.65	158	1.2
LoFTR	1.00	0.74	992	0.7

Table 2. Selection of results for **HPatches**.

Table 2 summarizes our results for the HPatches dataset. It shows that SIFT+FLANN are comparable to the learnable methods, and the FLANN *matcher* leads to only a few wrong matches, whereas especially ORB+NN shows worse results and a high amount of outliers in the matches. The AUC of the homography error up to five pixels is similar but not identical to the values given in the literature for SuperPoint(SP)+SuperGlue(SG) and SuperPoint+LightGlue(LG)<sup>7</sup> and for LoFTR (Sun et al., 2021).

Model	mPrec. @1e-3	AUC @5/10/20°	Time [s/pair]
SIFT+FLANN	0.70	0.31/0.45/0.58	0.41
ORB+NN	0.24	0.08/0.15/0.25	0.10
AKAZE+NN	0.27	0.13/0.24/0.38	0.28
SP+SG	0.77	0.48/0.65/0.79	0.48
SP+LG	0.80	0.51/0.68/0.81	0.39
DISK+LG	0.86	0.46/0.63/0.76	1.20
LoFTR	0.61	0.35/0.55/0.71	0.73

Table 3. Selection of results for **Megadepth-1500**.

For the Megadepth-1500 evaluation, we provide a selection of metrics in Table 3. For this dataset, the learnables clearly outperform the handcrafted methods. The differences between the methods were now more distinct, with again ORB+NN and AKAZE+NN showing the lowest, SIFT+FLANN an intermediate, and the learnables the highest performance in the order

<sup>7</sup> Results for SuperPoint+SuperGlue and SuperPoint+LightGlue using the OpenCV RANSAC estimator are given in the GlueFactory repository <https://github.com/cvg/glue-factory>. The values in the article (Lindenberg et al., 2023) are different since they are computed using MAGSAC for outlier removal.

LoFTR, DISK+LightGlue, SuperPoint+SuperGlue, and SuperPoint+LightGlue respectively. Again, the NN-*matcher* based methods have a high percentage of outliers. However, the runtime of the binary features ORB and AKAZE is still favourable compared to the learnable methods, even though they were paired with the computationally intense nearest-neighbour search. Again, our values for the AUC of the relative pose error at the thresholds of 5/10/20° for SuperPoint combined with SuperGlue and Lightglue were in the same range but not identical to (Lindenberg et al., 2023).

We also recorded instances where the models performed differently than in the literature. For DISK, we recorded unusually high runtimes which were inconsistent with the values given, e.g., by Lindenberg et al. (2023). The other method with unexpected behaviour is LoFTR. The dense *matcher* should outperform the two-step methods ((Sun et al., 2021), (Lindenberg et al., 2023)). However, our AUCs on Megadepth-1500 were considerably lower than the ones in the literature (Sun et al., 2021; Lindenberg et al., 2023). The difference might be due to the implementation being used from Kornia instead of the original code or by different resizing parameters.

## 5.2 Results for the custom image-model pairs

We evaluated the results on our first custom image-model car dataset (Table 4). The AUCs were now given separately for the translation error and the rotation error. Even though the results were limited by the difficulty of the matching task and geometric estimation as well as the inconsistencies of the datasets, they still shown differences in the performance of the methods. Whereas the handcrafted methods failed completely, the learnables were still able to cope to a certain degree. SuperGlue+LightGlue performs best under these challenging conditions. The results for our second custom dataset of image-model

Model	mPrec. @ 30px	AUC @ 3°	AUC @ 1m	mInl.
SIFT+FLANN	0.019	0.002	0.007	0
ORB+NN	0.004	0.000	0.000	0
AKAZE+NN	0.004	0.000	0.000	0
SP+SG	0.146	0.108	0.081	3
SP+LG	0.247	0.155	0.090	12
DISK+LG	0.295	0.093	0.081	11
LoFTR	0.153	0.088	0.050	6

Table 4. Selection of results for **TUM car-texture**.

UAV images are shown in Table 5. As the number of pairs is relatively small for this one, the results might not be as representative as the car dataset. However, the UAV-based acquisition introduces a new perspective and stronger intensity changes due to shadows (Figure 7). The even more challenging nature of the UAV-texture pairs is also reflected in the results. Again, the classical methods fail in all cases, and the learnable methods are partially unable to match the images. Again, the best performance is provided by the SuperPoint+LightGlue combination. Figure 7 illustrates our observation that for our buildings datasets with oblique views, repetitive structures, and small portions of overlap, the usage of a method with a keypoint extractor plus attention-based matching as used by SuperPoint+LightGlue and SuperPoint+SuperGlue seems promising.

Model	mPrec. @ 30px	AUC @ 3°	AUC @ 5m	mInl.
SIFT+FLANN	0.000	0.000	0.000	0
ORB+NN	0.003	0.000	0.000	0
AKAZE+NN	0.000	0.000	0.000	0
SP+SG	0.073	0.076	0.090	3
SP+LG	0.111	0.093	0.126	3
DISK+LG	0.008	0.076	0.035	0
LoFTR	0.019	0.038	0.040	5

Table 5. Selection of results for **TUM UAV-texture**.

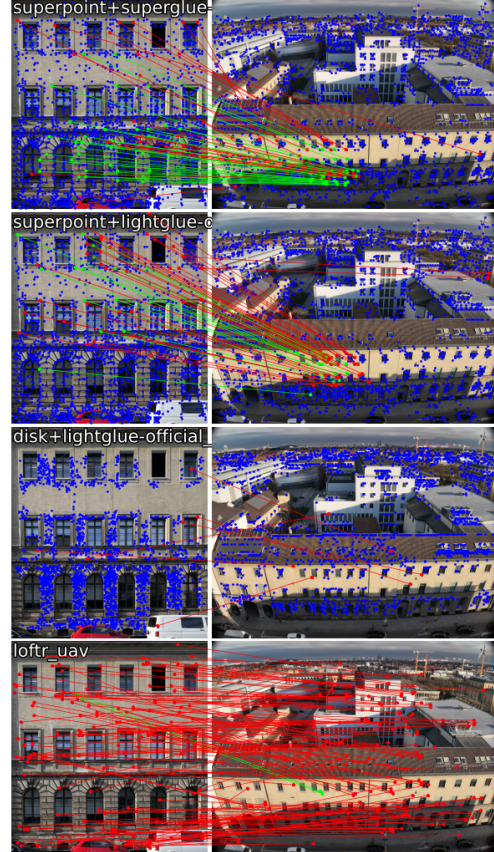


Figure 7. Example for learnables UAV-image-to-texture keypoints (blue), matches (red) and matches below re-projection error threshold of 30 px (green).

## 6. Discussion

In the following, we point out some limitations of our proposed feature matching evaluation with textures from semantic CityGML building models and camera images.

With the fast developments in deep learning on images, our selection of methods is already quite restricted with only pure feature matching methods. The recent, more general frameworks such as MAST3R (Leroy et al., 2024) and VGGT (Wang et al., 2025), where two-view image matching is only one by-product, might also be promising for our application in the future.

One limitation of using the learnables on our custom datasets is the domain shift from projective geometry to orthorectified texture images. However, as no training data is available, we have to rely on the pre-trained models and rely on their generalization capability.

One drawback of the coarse LoD2 models is the limited accuracy of the computed world coordinates for texture image locations. All objects that are out of the facade's plane have an error in their assumed world coordinates, depending on their geometry. For example, in Figure 6, the roofing and certain facade parts do not lie in the planar facade face. If the number of out-of-plane matches is large, the pose estimation will certainly deteriorate.

Another drawback yet to be solved are the dataset inconsistencies. As the image data was collected from different sources, they do not align perfectly. Even though all involved datasets are in absolute coordinates (UTM projection + height), the individual datasets differ within the range of decimeters. This is exemplarily visualized in Figure 8, which shows the edges of the facade face from the CityGML file together with the car and UAV point clouds colored in the point-to-facade-plane distance.

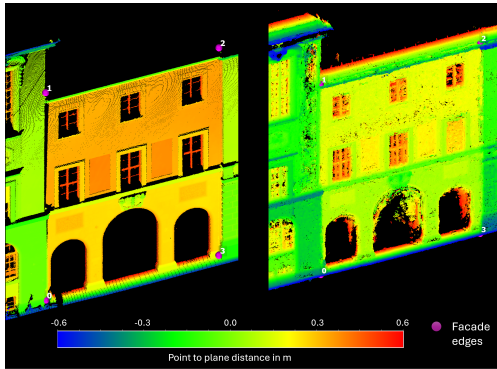


Figure 8. Car and UAV point cloud and facade edges (pink circles), colored in point to plane distance.

Figure 8 shows the decimeter-range differences in the edge positions as well as in the facade planes. This explains, at least partially, why our estimated poses differ in a similar magnitude from the ground truth and the re-projection error is in the range of tens of pixels even when the matching is successful. Figure 9 illustrates the re-projection errors using the ground truth pose for manually picked matching points in the image and the facade.

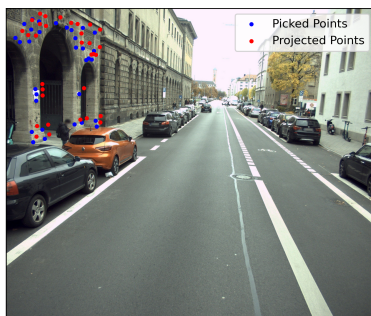


Figure 9. Error between manually picked points and projected, corresponding facade points using ground truth pose.

Figure 9 illustrates the re-projection errors using the ground truth pose for manually picked matching points in the image and the facade.

Another limitation of our method is the challenging geometry for estimating the pose. Especially for some car images, the keypoints are expected to be ill-distributed in the image due to oblique views and the limited extent of the facade in the image (Figure 9). Furthermore, our keypoints are restricted to a planar

scene, which might be unfavourable for the PnP algorithm. One solution could be to include the textures of several faces.

## 7. Conclusion

Our experiments confirm that the investigated learnable pipelines for feature extraction and matching perform better than the handcrafted ones. Our evaluation suggests that among the learnable methods, SuperPoint+SuperGlue and SuperPoint+Lightglue perform better on our challenging custom dataset, whereas the handcrafted methods show limited performance.

Since it is possible to determine correspondences between the facade textures and a query image, the textured models can be used for positioning with prior knowledge of the viewed buildings. However, due to the simple models and their unknown accuracy, this might only work for coarse or relative positioning. Given that the goal is to derive highly accurate absolute poses from the models, a thorough survey of their quality and the reliability of the ground truth poses of our datasets needs to be done beforehand.

Future mobile mapping applications could investigate whether matched world coordinates from the facades can successfully be used as landmarks for SLAM-based positioning of the car or the UAV. Another direction could be to compare the visual localization capabilities of our direct texture-image-to-image approach to other methods, e.g., rendered-model-image-to-image or using different model types as reference.

## Acknowledgements

This work was conducted within the framework of the Leonhard Obermeyer Center. We thank Sebastian Tutas and 3D Mapping Solutions GmbH for providing car-dataset and valuable support. We also acknowledge the creators of the GlueFactory repository for their contributions to the tools used in this study.

## References

- Alcantarilla, P. F., Solutions, T., 2011. Fast explicit diffusion for accelerated features in nonlinear scale spaces. *IEEE Trans. Patt. Anal. Mach. Intell.*, 34(7), 1281–1298.
- Anders, K., Wang, J., Wysocki, O., Huang, X., Liu, S., 2025. Uav laser scanning and photogrammetry of tum downtown campus.
- Arandjelović, R., Zisserman, A., 2012. Three things everyone should know to improve object retrieval. *2012 IEEE conference on computer vision and pattern recognition*, IEEE, 2911–2918.
- Balntas, V., Lenc, K., Vedaldi, A., Mikolajczyk, K., 2017. Hpatches: A benchmark and evaluation of handcrafted and learned local descriptors. *Proceedings of the IEEE conference on computer vision and pattern recognition*, 5173–5182.
- Bay, H., Tuytelaars, T., Van Gool, L., 2006. Surf: Speeded up robust features. *Computer Vision–ECCV 2006: 9th European Conference on Computer Vision, Graz, Austria, May 7–13, 2006. Proceedings, Part I 9*, Springer, 404–417.
- Bian, J., Yang, R., Liu, Y., Zhang, L., Cheng, M., Reid, I. D., Wu, W., 2018. MatchBench: An Evaluation of Feature Matchers. *CoRR*, abs/1808.02267. <http://arxiv.org/abs/1808.02267>.

- Bieringer, A., Wysocki, O., Tuttas, S., Hoegner, L., Holst, C., 2024. Analyzing the Impact of Semantic LoD3 Building Models on Image-based Vehicle Localization. *ISPRS Annals of the Photogrammetry, Remote Sensing and Spatial Information Sciences*, 10, 55–62.
- DeTone, D., Malisiewicz, T., Rabinovich, A., 2018. Superpoint: Self-supervised interest point detection and description. *Proceedings of the IEEE conference on computer vision and pattern recognition workshops*, 224–236.
- Gröger, G., Kolbe, T. H., Nagel, C., Häfele, K.-H., 2012. Ogc city geography markup language (citygml) encoding standard.
- Huang, Q., Guo, X., Wang, Y., Sun, H., Yang, L., 2024. A survey of feature matching methods. *IET Image Processing*, 18(6), 1385–1410.
- Karpur, A., Perrotta, G., Martin-Brualla, R., Zhou, H., Araujo, A., 2024. Lfm-3d: Learnable feature matching across wide baselines using 3d signals. *Proc. 3DV'24*.
- Kolbe, T. H., Donaubaue, A., 2021. Semantic 3D city modeling and BIM. W. Shi, M. F. Goodchild, M. Batty, M.-P. Kwan, A. Zhang (eds), *Urban Informatics*, Springer Singapore, Singapore, 609–636.
- Leroy, V., Cabon, Y., Revaud, J., 2024. Grounding image matching in 3d with mast3r.
- Li, S., Xu, C., Xie, M., 2012. A robust  $O(n)$  solution to the perspective-n-point problem. *IEEE transactions on pattern analysis and machine intelligence*, 34(7), 1444–1450.
- Li, Z., Snavely, N., 2018. Megadepth: Learning single-view depth prediction from internet photos. *Proceedings of the IEEE conference on computer vision and pattern recognition*, 2041–2050.
- Lin, T.-Y., Maire, M., Belongie, S., Hays, J., Perona, P., Ramanan, D., Dollár, P., Zitnick, C. L., 2014. Microsoft coco: Common objects in context. *Computer vision—ECCV 2014: 13th European conference, zurich, Switzerland, September 6–12, 2014, proceedings, part v 13*, Springer, 740–755.
- Lindenberger, P., Sarlin, P.-E., Pollefeys, M., 2023. Lightglue: Local feature matching at light speed. *Proceedings of the IEEE/CVF International Conference on Computer Vision*, 17627–17638.
- Loeper, Y., Gerke, M., Alamouri, A., Kern, A., Bajauri, M. S., Fanta-Jende, P., 2024. Visual localization in urban environments employing 3D city models. *The International Archives of the Photogrammetry, Remote Sensing and Spatial Information Sciences*, 48, 311–318.
- Lowe, D. G., 2004. Distinctive image features from scale-invariant keypoints. *International journal of computer vision*, 60, 91–110.
- Mueller, M. S., Sattler, T., Pollefeys, M., Jutzi, B., 2019. Image-to-image translation for enhanced feature matching, image retrieval and visual localization. *ISPRS annals*, IV-2/W7, 111–119.
- Muja, M., Lowe, D. G., 2009. Fast approximate nearest neighbors with automatic algorithm configuration. *VISAPP (1)*, 2(331–340), 2.
- Panek, V., Kukulova, Z., Sattler, T., 2022. Meshloc: Mesh-based visual localization. *European Conference on Computer Vision*, Springer, 589–609.
- Panek, V., Kukulova, Z., Sattler, T., 2023. Visual localization using imperfect 3d models from the internet. *Proceedings of the IEEE/CVF Conference on Computer Vision and Pattern Recognition*, 13175–13186.
- Pautrat, R., Suárez, I., Yu, Y., Pollefeys, M., Larsson, V., 2023. GlueStick: Robust Image Matching by Sticking Points and Lines Together. *International Conference on Computer Vision (ICCV)*.
- Riba, E., Mishkin, D., Ponsa, D., Rublee, E., Bradski, G., 2020. Kornia: an open source differentiable computer vision library for pytorch. *Proceedings of the IEEE/CVF Winter Conference on Applications of Computer Vision*, 3674–3683.
- Rublee, E., Rabaud, V., Konolige, K., Bradski, G., 2011. Orb: An efficient alternative to sift or surf. *2011 International conference on computer vision*, Ieee, 2564–2571.
- Sarlin, P.-E., DeTone, D., Malisiewicz, T., Rabinovich, A., 2020. Superglue: Learning feature matching with graph neural networks. *Proceedings of the IEEE/CVF conference on computer vision and pattern recognition*, 4938–4947.
- Sattler, T., Maddern, W., Toft, C., Torii, A., Hammarstrand, L., Stenborg, E., Safari, D., Okutomi, M., Pollefeys, M., Sivic, J. et al., 2018. Benchmarking 6dof outdoor visual localization in changing conditions. *Proceedings of the IEEE conference on computer vision and pattern recognition*, 8601–8610.
- Schönberger, J. L., Frahm, J.-M., 2016. Structure-from-motion revisited. *Conference on Computer Vision and Pattern Recognition (CVPR)*.
- Sun, J., Shen, Z., Wang, Y., Bao, H., Zhou, X., 2021. Loft: Detector-free local feature matching with transformers. *Proceedings of the IEEE/CVF conference on computer vision and pattern recognition*, 8922–8931.
- Tyszkiewicz, M., Fua, P., Trulls, E., 2020. DISK: Learning local features with policy gradient. *Advances in Neural Information Processing Systems*, 33, 14254–14265.
- Wang, J., Chen, M., Karaev, N., Vedaldi, A., Rupprecht, C., Novotny, D., 2025. Vggt: Visual geometry grounded transformer.
- Wysocki, O., Schwab, B., Beil, C., Holst, C., Kolbe, T. H., 2024. Reviewing Open Data Semantic 3D City Models to Develop Novel 3D Reconstruction Methods. *The International Archives of the Photogrammetry, Remote Sensing and Spatial Information Sciences*, 48, 493–500.
- Wysocki, O., Schwab, B., Biswanath, M. K., Greza, M., Zhang, Q., Zhu, J., Froeh, T., Heeramaglore, M., Hijazi, I., Kanna, K., Pechinger, M., Chen, Z., Sun, Y., Segura, A. R., Xu, Z., AbdelGafar, O., Mehranfar, M., Yeshwanth, C., Liu, Y.-C., Yazdi, H., Wang, J., Auer, S., Anders, K., Bogenberger, K., Borrmann, A., Dai, A., Hoegner, L., Holst, C., Kolbe, T. H., Ludwig, F., Nießner, M., Petzold, F., Zhu, X. X., Jutzi, B., 2025. TUM2TWIN: Introducing the Large-Scale Multimodal Urban Digital Twin Benchmark Dataset. *arXiv preprint arXiv:2505.07396*.
- Xu, S., Chen, S., Xu, R., Wang, C., Lu, P., Guo, L., 2024. Local feature matching using deep learning: A survey. *Information Fusion*, 107, 102344.